Korean J. Chem. Eng., 33(5), 1534-1550 (2016)
DOI: 10.1007/s11814-015-0281-x

pISSN: 0256-1115
eISSN: 1975-7220

Heat transfer and fluid flow modeling in serpentine microtubes using adaptive neuro-fuzzy approach

Reza Beigzadeh, Marziyeh Hajialyani, and Masoud Rahimi†

CFD Research Center, Chemical Engineering Department, Razi University, Kermanshah, Iran
(*Received 29 August 2015 • accepted 11 December 2015*)

Abstract−An adaptive neuro-fuzzy inference system (ANFIS) is applied to predict thermal and flow characteristics in serpentine microtubes. Heat transfer rate and pressure drop were experimentally measured for six serpentine microtubes with different geometrical parameters. Thermal and flow characteristics were obtained in various flow conditions. The ANFIS models were trained using the experimental data to predict Nusselt number (Nu) and friction factor (f) in the studied serpentine microtubes as a function of geometric parameters and flow conditions. The model was validated through testing data set, which were not previously introduced to the developed ANFIS. For Nu prediction, the root mean square error (RMSE), mean relative error (MRE), and absolute fraction of variance (R^2) between the predicted results and experimental data were found 0.2058, 1.74%, and 0.9987, respectively. The corresponding calculated values for f were 0.0056, 2.98%, and 0.9981, respectively. The prediction accuracy of the ANFIS models was compared with that of corresponding classical power-law correlations and its advantages are illustrated.

Keywords: Heat Transfer, Pressure Drop, Serpentine Microtubes, ANFIS, Modeling

INTRODUCTION

The rapid development in microscale devices has led to rapid expansion of applied research in micro-fluidic systems in the field of microchannels and microtubes. They are the essential elements for transporting fluid within a miniature area. Broadly, the designs and the process controls of micro-fluidic systems are affected by the impact of geometrical configurations on the fluid flow characteristics such as temperature, pressure, and velocity distributions in the micrometer scale. Usually the flow regime in micro-channels is laminar and the laminar flow and development of boundary layers (velocity and thermal) causes the reduction of heat transfer performance. Different types of active and passive methods are applied for breaking the boundary layers. Using channels with serpentine configuration is one of the passive methods for enhancing the heat transfer rate. Therefore, for optimal design and process control of micro-fluidic devices, it is quite useful to predict the fluid flow and heat transfer characteristics in microchannels, including straight and serpentine microchannels. Experimental and numerical research on heat transfer and fluid flow in straight microchannels has been extensively conducted, based on several literature reviews [1-4]. One of the first investigations on straight circular microtube was by Choi et al. [5]. They studied the heat transfer and pressure drop features of nitrogen gas in three silica microtubes with different inner diameters. They concluded that the dependence of Nusselt number on Reynolds number in microtubes is different from the macroscale theory. The critical Reynolds number was 2000, which is coincident with this number for macrotube. Hong and Asako [6] numerically investigated the heat transfer characteristics of gaseous flow in micro-channels and microtubes based on the Arbitrary Lagrangian-Eulerian (ALE) method. They proposed a correlation for prediction of the wall temperature of gaseous flow in microtubes. Many other studies have been conducted on the flow characteristics and heat transfer in straight microtubes [7-10]. There is limited literature that focuses on fluid flow characteristics in serpentine configuration. The serpentine configuration is comprised of bend section with repeating units. The formation of secondary flows (Dean vortices) in bends, due to centrifugal force, can increase the pressure drop and heat transfer relative to similar flows in straight microtubes. The pressure drop penalty is much smaller than heat transfer enhancement. For the first time, Dean [11,12] studied the Dean vortices for a coiled tube with constant curvature. Many researchers have employed this mechanism for heat transfer enhancement. Patankar et al. [13] examined the effect of the secondary flow on friction factor and heat transfer in the helically coiled pipes. Kalb and Seader [14] conducted a numerical investigation on the effect of Dean vortices on the fully developed heat transfer of viscous flow in curved circular tubes. Sui et al. [15,16] used three-dimensional conjugate simulation based on the classical continuum approach to study the flow in wavy micro-channels with a rectangular cross section. A good agreement was found between the experimental and the numerical results. Some investigations appraised the performance of liquid flow through the serpentine channels with various cross-sections [17-21]. They concluded that the vortical flow patterns near the bends emerge with increasing Reynolds number. They showed that domination of flow area by these vortices caused an efficient fluid mixing and heat transfer rate enhancement.

Nevertheless, in thermal systems, improving the heat transfer performance is generally associated with increase in pressure drop.

†To whom correspondence should be addressed.
E-mail: masoudrahimi@yahoo.com, m.rahimi@razi.ac.ir

This causes increasing the pumping power requirement, which is inappropriate due to higher consumption of energy. Eliminating this drawback is more important for microchannels due to high pressure drop in the microscale devices. Therefore, reliable estimation models can be employed to optimize the operational conditions.

The artificial neural network (ANN) based models with their large parameters (weights and biases) have been successfully employed for modeling of non-linear complicated systems. This ability has been especially characterized in the development of models that are based on the experimental data. ANNs can learn and recognize knowledge and rules beyond the experimental data using their learning process. Neural networks applying nonlinear methods, and when employed for modeling the nonlinear data, may estimate such data with a greater accuracy in comparison with other models. Jang [22] proposed the combination of ANNs and fuzzy systems, which is known as adaptive neuro-fuzzy inference system (ANFIS). This combination creates an efficient model which uses the characteristics of the two approaches and enhances the performance of the neuro-fuzzy system. Mohanraj et al. [23] reviewed the applications of artificial neural networks for investigating the energy and exergy in refrigeration, air-conditioning and heat pump (RACHP) systems. They illustrated that ANN can be successfully employed in the field of RACHP systems with suitable precision. The combination of ANN with other expert systems such as genetic algorithms and fuzzy logic indicated better performance compared with typical ANN modeling. In addition, Mohanraj et al. [24] provided a literature review on application of ANFIS for modeling in field of heat transfer processes. Mirsepahi et al. [25] developed ANN and ANFIS techniques for inverse heat transfer modeling of an irradiative batch dryer. These approaches were used for the prediction of the required input power in the investigated irradiative dryer, and the results of each model were compared. Beigzadeh and Rahimi [26] investigated the application of ANFIS technique for estimating the heat transfer and friction characteristics in helically coiled tube heat exchangers. They compared modeling results with experimental data and reported the prediction of experimental data with high accuracy. In addition, they compared the model with ANN and empirical correlations. Mehrabi and Pesteei [27] proposed an adaptive neuro-fuzzy inference system for estimating the heat transfer rate of supercritical carbon dioxide turbulent flow in a vertical tube. They reported the high ability of the developed model for prediction of the experimental data.

This study aims to present a model for estimation of heat transfer performance in microtubes with a serpentine configuration. There are various types of serpentine configurations, based on the bend geometry and presence or absence of straight portions. Due to this diversity, investigating the effect of geometrical characteristics and providing reliable prediction models are essential for selection of the optimal geometrical configuration and parameters. In this study, two adaptive neuro-fuzzy inference systems were developed to predict thermal and hydrodynamics characteristics in serpentine microtubes. The experimental data related to serpentine

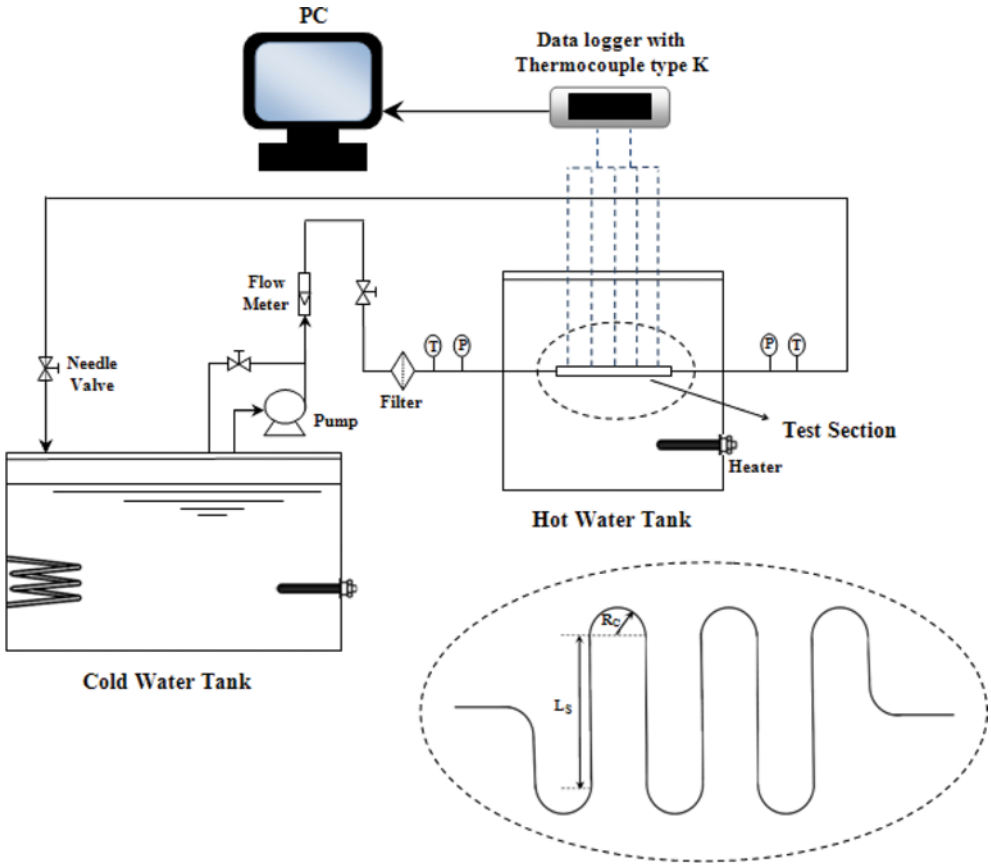

Fig. 1. Schematic diagram of the experimental setup.

microtubes with different geometric parameters (curvature radius and straight length between bends) were used for developing the models. In the model, Nusselt number (Nu) and friction factor (f) are the target (output) data.

EXPERIMENTAL PROCEDURE

1. Test Section

A schematic of a serpentine microtube with its main geometric parameters is depicted in Fig. 1. R_C is the curvature radius, and L_S is the straight length between bends. We used six copper microtubes with an inner diameter of 787.4 μm. To examine the effect of curvature radius and straight length between bends, serpentine microtubes with different curvature radiuses (0.75, 1, 1.25, and 1.5 cm) and straight lengths (1, 2.5, and 5 cm) were employed. The dimensions of the serpentine microtubes are listed in Table 1. As an example, a real serpentine microtube with R_C=1 and L_S=1 is shown in Fig. 2. Turning to Fig. 1, the experimental facility is composed of the test section, the water driven system, and the data acquisition section. Distilled water from a reservoir was driven through the test section using a pump. The flow through the system was controlled by two needle valves. To prevent the flow blocking from small particles and contaminants, a filter was adjusted before the test section. The water subsequently entered the test section. The test section contained a microtube immersed in a bath. The temperature of the bath was kept constant during the tests using a temperature controller. The fluid temperature increases due to absorbing the heat from the bath, when passing through the microtube. Five K-type thermocouples were installed at three specific points on the surface of each microtube to measure the wall temperature. Two thermocouples were also installed at the inlet and outlet of the microtubes to measure the water temperature at the inlet and outlet of the test section. The thermocouples were connected to a digital thermometer (Lutron, BTM-4208SD) to record the temperatures. To measure the upstream and downstream pressure, two pressure transducers were installed at the inlet and outlet of micro-channels. They sent the measured pressures to the data acquisition system. The properties of water used in these experiments were determined in the bulk temperature of fluid (the average of inlet and outlet temperature). In all experiments, the system was permitted to run for a long enough time to ensure steady-state conditions and all measured data were recorded when pressure and temperature remained unchanged or those fluctuations were very small. Then, they were transmitted to a PC to process and analyze the measured data.

Table 1. Details of the employed serpentine micro tubes

Geometry number	R_C, cm	L_S, cm	L, cm	R_C/d	L_C/d
1	0.75	5	49.87	9.525	63.50
2	1	5	56.89	12.700	63.50
3	1.25	5	55.13	15.875	63.50
4	1.5	5	63.86	19.050	63.50
5	1	2.5	36.96	12.700	31.75
6	1	1	34.84	12.700	12.70

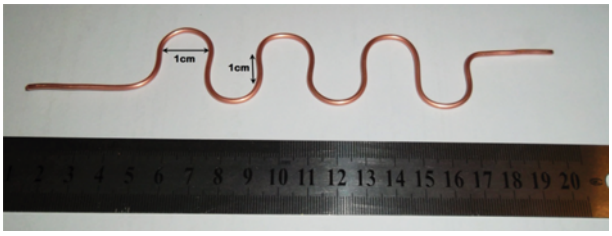

Fig. 2. Serpentine microtube (R_C=1 and L_S=1).

2. Calculation of Nusselt Number and Friction Factor

To express the experimental results in a more efficient way, the measured data were diminished using following relations. Reynolds number was calculated as follows:

$$\mathrm{Re}=\frac{\rho \mathrm{V} \mathrm{d}_i}{\mu} \tag{1}$$

where, V is the mean flow velocity, ρ and μ are the fluid density and dynamic viscosity, respectively, and d_i is the inner microtube diameter.

The measured pressure drop was used to evaluate the fluid friction factor, based on Eq. (2):

$$\Delta \mathrm{P}=\frac{\rho \mathrm{V}^2}{2}\left(\mathrm{f}\frac{\mathrm{L}}{\mathrm{d}_i}+\sum \mathrm{K}_L\right) \tag{2}$$

where f is the friction factor, ΔP is the measured pressure drop; L is the microtube length, and $\sum K_L$ is defined as the sum of minor losses due to the inlet, outlet, change in diameter, etc. Minor losses were determined and were found to be negligible compared with the measured pressure drop. So, the friction factor can be found according to the following equation:

$$\mathrm{f}=2\frac{\Delta \mathrm{P} \mathrm{d}_i}{\rho \mathrm{V}^2 \mathrm{L}} \tag{3}$$

The heat transfer coefficient was calculated from the measured wall temperature. Due to the low resistance of the copper microtube wall, the temperature difference between inside and outside of the tube wall was assumed negligible. The added heat to the fluid can be calculated using the measured inlet temperature (T_i) and outlet temperature (T_o) of the fluid as follows:

$$\mathrm{Q}_a=\mathrm{MC}_p(\mathrm{T}_o-\mathrm{T}_i) \tag{4}$$

This value of heat transfer is equal to the convection heat transfer of fluid in the micro-tube:

$$\mathrm{Q}_a=\mathrm{Q}_{conv}=\mathrm{hA}(\mathrm{T}_b-\tilde{\mathrm{T}}_W) \tag{5}$$

In which, h is the average value of heat transfer coefficient, A is the internal surface of microtubes, T_b is the bulk temperature (the mean of inlet and outlet temperatures) and $\tilde{T}_W$ is the average surface temperature of the five measuring points as follows:

$$\mathrm{T}_b=\frac{\mathrm{T}_i+\mathrm{T}_o}{2} \text{ and } \tilde{\mathrm{T}}_W=\frac{\sum \mathrm{T}_W}{5} \tag{6}$$

Finally, the Nusselt number is expressed as follows:

$$Nu = \frac{h d_i}{k_f} \tag{7}$$

3. Uncertainty in Experimental Data

The major part of experimental errors resulted from the measuring apparatus, especially pressure, flow rate, and temperature. The accuracy of measuring apparatus was found 0.1 kPa for pressure transducers, 0.5 lit/min for flow meter, and 0.1 °C for temperature measuring instruments (thermocouples and Data logger). Based on the above values and according to uncertainty analysis presented by Holman [28], the uncertainty of Nu, f, and Re was calculated. Based on Holman analysis [28], if the given function, such as G, is a function of independent variables $x_1, x_2, \ldots, x_n$, and $\delta x_1, \delta x_2, \ldots, \delta x_n$ are the uncertainty of the variables, the uncertainty of the function can be determined using the following relation:

$$U_G = \sqrt{\left(\frac{\partial G}{\partial x_1}\right)^2 \delta x_1^2 + \left(\frac{\partial G}{\partial x_1}\right)^2 \delta x_1^2 + \cdots + \left(\frac{\partial G}{\partial x_n}\right)^2 \delta x_n^2} \tag{8}$$

where G is as follows:

$$G = x_1^{a_1} x_2^{a_2} \cdots x_n^{a_n} \tag{9}$$

U_G is obtained by the following relation:

$$\frac{U_G}{G} = \sqrt{\sum \left(\frac{a_i \delta x_i}{x_i}\right)^2} \tag{10}$$

According to the above analysis, the experimental uncertainties were calculated using the Eqs. (1-7). Finally, these expressions were produced for uncertainties of Re, f, and Nu as follows:

Table 2. Experimental errors based on instruments and methods

Parameter	$\delta\rho/\rho$	$\delta\mu/\mu$	$\delta k_f/k_f$	$\delta C_p/C_p$	$\delta d_i/d_i$	$\delta L/L$
Experimental error	~2%	~2%	~1%	~2.5%	~3%	~1%

$$\frac{U_{Re}}{Re} = \sqrt{\left(\frac{\delta\rho}{\rho}\right)^2 + \left(\frac{\delta\mu}{\mu}\right)^2 + \left(\frac{\delta d_i}{d_i}\right)^2 + \left(\frac{\delta M}{M}\right)^2} \tag{11}$$

$$\frac{U_f}{f} = \sqrt{\left(\frac{\delta\rho}{\rho}\right)^2 + \left(\frac{\delta\Delta P}{\Delta P}\right)^2 + 4\left(\frac{\delta M}{M}\right)^2 + 9\left(\frac{\delta d_i}{d_i}\right)^2 + \left(\frac{\delta L}{L}\right)^2} \tag{12}$$

$$\frac{U_{Nu}}{Nu} = \sqrt{\begin{array}{l}\left(\frac{\delta\rho}{\rho}\right)^2 + \left(\frac{\delta C_p}{C_p}\right)^2 + \left(\frac{\delta k_f}{k_f}\right)^2 + \left(\frac{\delta M}{M}\right)^2 + \left(\frac{\delta L}{L}\right)^2 \\ + \left(\frac{\delta(T_o - T_i)}{(T_o - T_i)}\right)^2 + \left(\frac{\delta(T_b - \tilde{T}_w)}{(T_b - \tilde{T}_w)}\right)^2\end{array}} \tag{13}$$

The uncertainties of above parameters are given in the Table 2. The values reported in this table indicate that all the uncertainty values are suitable and the measurements have satisfactory precision. The average uncertainty for Re, f, and Nu was found 4.1%, 6.3%, and 7%, respectively.

MODELING STUDY

1. Neural Networks and Adaptive Neuro-fuzzy Inference Systems

Applications of analytic computer codes for the engineering

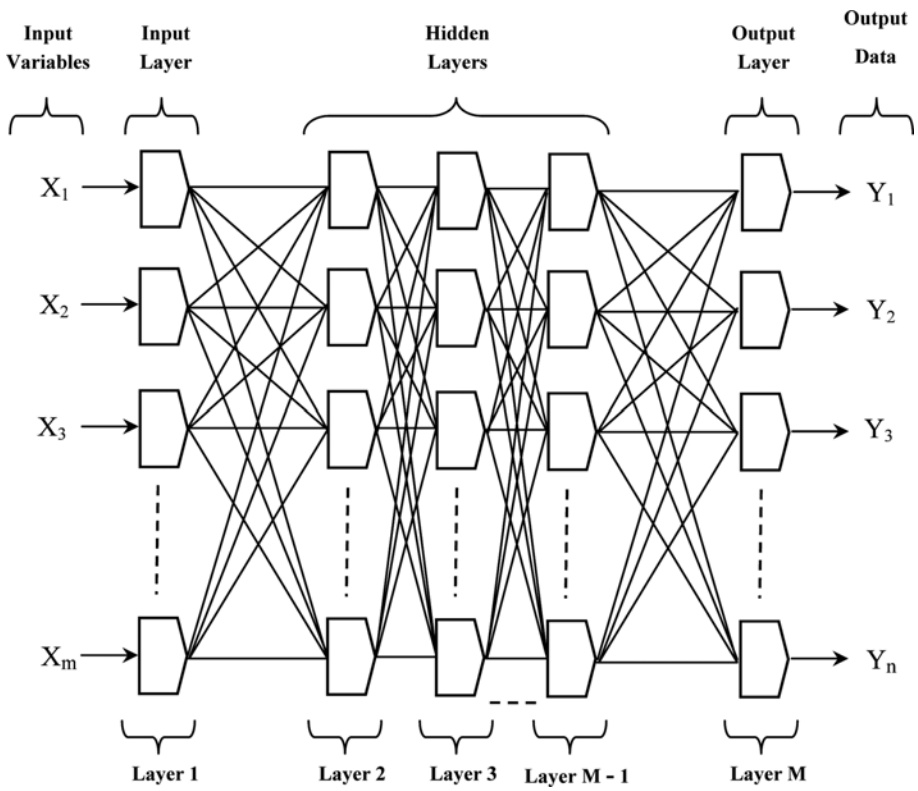

Fig. 3. Multilayer feed-forward ANN architecture.

systems are usually time consuming and complicated, due to the necessity of solving complex differential equations. Therefore, artificial neural network (ANNs) techniques using the 'learning' capability (by training data) can be very useful and appropriate for these systems. ANNs mimic biological nervous systems (i.e., biological neural network of the human brain) and can learn and recognize complicated relationships. They are comprised of a large number of simple processing units (neurons), which are in the interconnected structure to create a network with a set of weights and biases. These parameters (weights and biases) are modified during the learning process and produce a response for related input. The ANN parameters will be corrected systematically, until the overall errors between ANN output and target (experimental) data are less than the desired error value [29,30]. Generally, ANNs are regular structures including input layer of neurons, output layer, and hidden layers which are located between them. Fig. 3 illustrates a schematic structure of a multilayer feed-forward ANN in which input information is fed forward recursively toward next hidden layers, and lastly to the output layer. A supervisor instructs this type of the ANN to learn the relationships between the independent (input) and dependent (output) variables. ANNs has been highly recommended as a technique offering an alternative approach to predict the performance of engineering systems. Artificial neural networks and fuzzy systems are subsets of artificial intelligence systems. The ANNs are a low-level computational arrangement that create a relationship between input and output with raw data and they do not reveal logical relationships between main system components. Fuzzy logic systems work using reasoning and have higher level of computational structures. Nevertheless, a fuzzy system does not have the learning ability and consequently cannot adjust its components. A neuro-fuzzy system combines neural network and fuzzy system, using the advantages of the two approaches. One of the most powerful neuro-fuzzy systems, which have been proposed by Jang [22], is called as adaptive Neuro Fuzzy Inference System (ANFIS). The components of the ANFIS (i.e., fuzzy rules and membership functions) can be adjusted using the learning process and the model is used for approximating nonlinear relations.

2. Architecture of ANFIS

ANFIS is a fuzzy logic system in the structure of artificial neural networks. ANFIS employs two fuzzy logic and ANN techniques, which may lead to results comprising the advantages of both methods. The major aim of the ANFIS is to find a model that can estimate target data from the related inputs with a desired accuracy. The ANFIS model includes two sections (antecedent and conclusion) linked to each other by using a set of TSK type fuzzy if-then rules, in the network structure. This model can be used for predicting the nonlinear systems with a high precision due to its flexible mathematical structure.

For a Sugeno fuzzy inference system with two inputs (x and y) and one output (F) the fuzzy rules can be expressed as follows:

$$\text{Rule 1: If (x is } A_1\text{) and (y is } B_1\text{) then } F_1=p_1x+q_1y+r_1 \tag{14}$$

$$\text{Rule 2: If (x is } A_2\text{) and (y is } B_2\text{) then } F_2=p_2x+q_2y+r_2 \tag{15}$$

where p_i, q_i and r_i are linear output parameters and determined through the training procedure. A_i and B_i are fuzzy sets. The reasoning mechanism for two input Sugeno fuzzy system is shown in Fig. 4. A schematic of the equivalent ANFIS configuration is depicted in Fig. 5. As illustrated in Fig. 5, the ANFIS architecture includes five layers such as fuzzy, product, normalized, defuzzy, and total output layer. In the first layer (fuzzy layer) each node i has membership functions (MFs) in the fuzzy set. The output of the nodes in this layer is the membership grade of the input variable. Usual membership functions such as triangular, trapezoidal, Generalized bell, Gaussian, combination Gaussian, and *ΠΠ*-shaped were used in the present study. In all these functions maximum is 1 and minimum is 0. For example, trapezoidal and Gaussian MFs (see Fig. 4) are defined as follows:

$$\mu_{A_i}(x)=\max\left(\min\left(\frac{x-a}{b-a}, 1, \frac{d-x}{d-c}\right), 0\right) \tag{16}$$

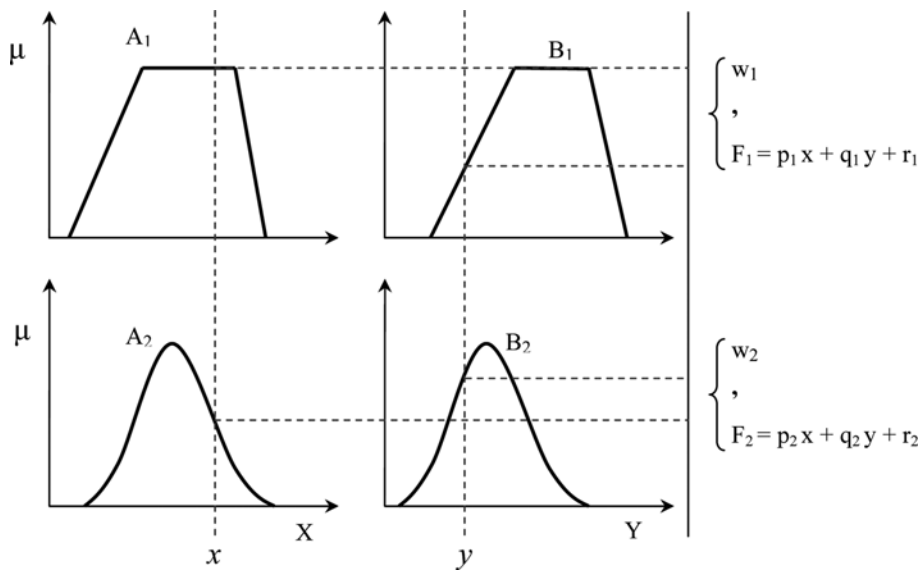

Fig. 4. The inference method of Sugeno FIS model with two rules and two inputs.

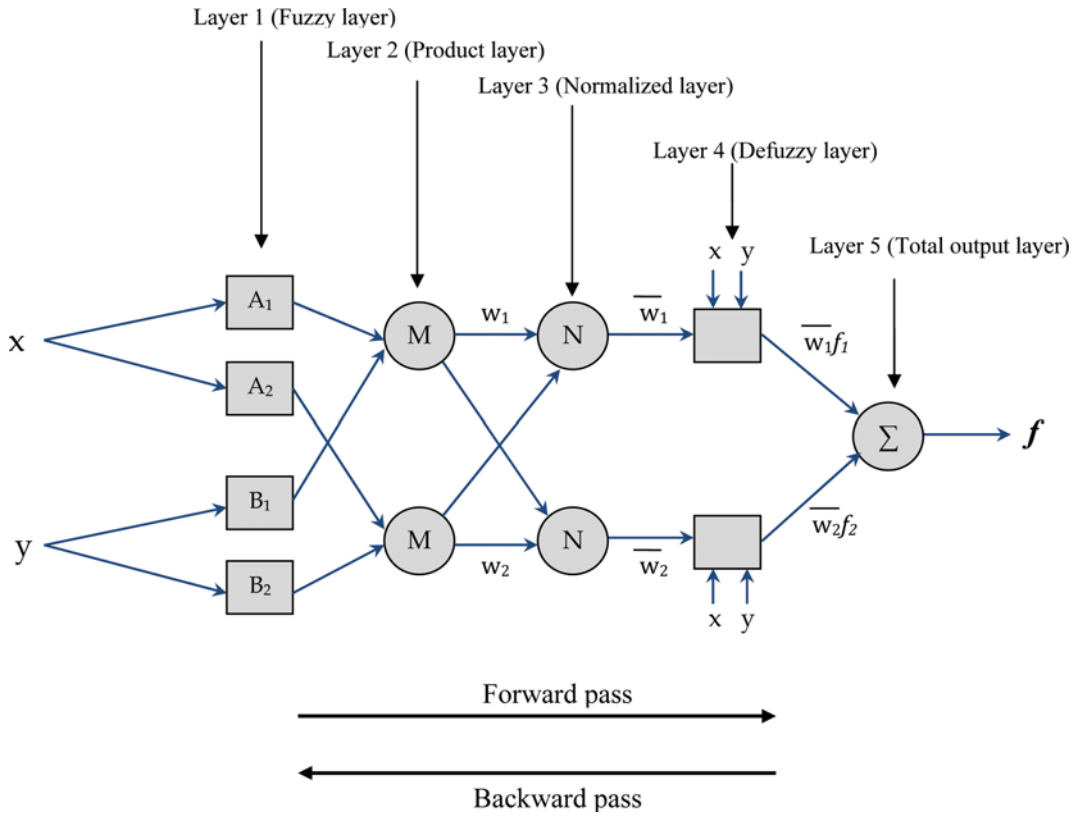

Fig. 5. Schematic view of adaptive neuro-fuzzy (ANFIS) model.

where a and d are located at the bottom of the trapezoid curve and the parameters b and c are located at the top.

$$\mu_{A_i}(x)=\exp\left[-\frac{1}{2}\left(\frac{x-m_i}{\sigma_i}\right)^2\right] \tag{17}$$

where m_i and σ_i are the Gaussian MF center and Gaussian MF width, respectively.

The output of this layer can be expressed as follows:

$$Q_{1,i}=\mu_{A_i}(x),\ \text{for i=1, 2} \tag{18}$$

Here x is the input value of the node i and $Q_{1,i}$ is the layer 1 output.

In layer 2 (product layer) the incoming signals into each fixed node are multiplied by each other and then the rule firing strength is provided. The output of the second layer, $Q_{2,i}$, is the product of the input signal values and is calculated as follows:

$$Q_{2,i}=w_i=\mu_{A_i}(x)\,\mu_{B_i}(y),\ \text{for i=1, 2} \tag{19}$$

μ_{A_i} is the membership grade of x in A_i fuzzy set and μ_{B_i} is the membership of y in fuzzy set of B_i.

In the third layer (normalized layer), which the nodes are denoted with "N", the normalized weight is calculated as follows:

$$Q_{3,i}=\overline{w}_i=\frac{w_i}{w_1+w_2},\ \text{for i=1, 2} \tag{20}$$

where $Q_{3,i}$ is the output of this layer which called normalized firing strength of *i*th rule.

Layer 4 is the defuzzy layer and the output of this layer ($Q_{4,i}$) is the specific function of inputs (x, y) multiplied by the normalized firing strength, which can be written as following relation (defuzzy relationship):

$$Q_{4,i}=\overline{w}_i f_i=\overline{w}_i(p_i x+q_i y+r_i),\ \text{for i=1, 2} \tag{21}$$

The linear parameters (p_i, q_i and r_i) are named consequent parameters and determined using the training process.

The single node of the last layer calculates the final decision or output of the ANFIS as follows:

$$Q_{5,i}=\sum_i \overline{w}_i f_i=\frac{\sum_i w_i f_i}{\sum_i w_i} \tag{22}$$

There are two types of adjustable parameters in the ANFIS structure, premise and consequent parameters, obtained by using the training procedure. The ANFIS parameters are modified in a two-step learning process for minimizing the error function [29]. The consequent parameters are adjusted using the least square estimation in forward pass, while the premise parameters are obtained using the gradient descend in backward pass [31]. Definitely, the more accurate selection of the optimum parameters gives the more accurate model. For the determination of the ANFIS configuration, grid partition and subtractive clustering methods were used. For using the grid partition technique, there are some MFs such as triangular, trapezoidal, Generalized bell, Gaussian, combination Gaussian, and *Π*-shaped. In this method, the MF type and number of the rules can be selected by trial-and-error scheme. In the subtractive clustering technique, data points are potential cluster centers and computing the amount of the probability of each data would define the cluster center based on the density of adjacent

data. For this method, four parameter values such as range of influence, squash actor, accepted ratio, and rejected ratio should be optimized. In this study, subtractive clustering parameters are determined by trial-and-error method.

This combination of the fuzzy logic and neural network leads to a powerful modeling tool for predicting the complex relationships. Furthermore, the ANFIS modeling achieves the desirable results in less time in comparison with ANN. Therefore, the ANFIS is a powerful approach for modeling and predicting the thermal systems. We tried to model the average Nusselt number (Nu) and friction factor (f) in the studied serpentine microtubes using two ANFIS approaches. The input parameters for the first ANFIS are Reynolds number (Re), Prandtl number (Pr), curvature ratio (R_C/d), and straight length to tube diameter ratio (L_S/d). In the second one, the friction factor is modeled with three input variables including Re, R_C/d, and L_S/d. Since all data values have different physical units and ranges, all data were normalized between zero and one to enhance the rate of computational process. The following relation was used for normalizing the input and output data values:

$$\text{Normalized data} = \frac{\text{data value} - \text{minimum value}}{\text{maximum value} - \text{minimum value}} \quad (23)$$

The hybrid-learning method was used for obtaining the parameters. The hybrid-learning method employs gradient method and least mean squares approximation to obtain the optimum parameters [22].

RESULTS AND DISCUSSION

1. General Observation

The ANFIS approaches were applied to model and predict the Nusselt number and friction factor in microtubes (inner diameter= 787.4 μm) with serpentine configurations. For input data, flow conditions (i.e. Re and Pr) and two main geometric parameters of the serpentine microtubes include curvature radius (R_C) and straight length between bends (L_S) in the dimensionless form (R_C/d, L_S/d) were chosen. Therefore, the heat transfer rate and pressure drop in the examined serpentine microtubes were measured using designed experimental setup. Consequently, the influences of the geometric

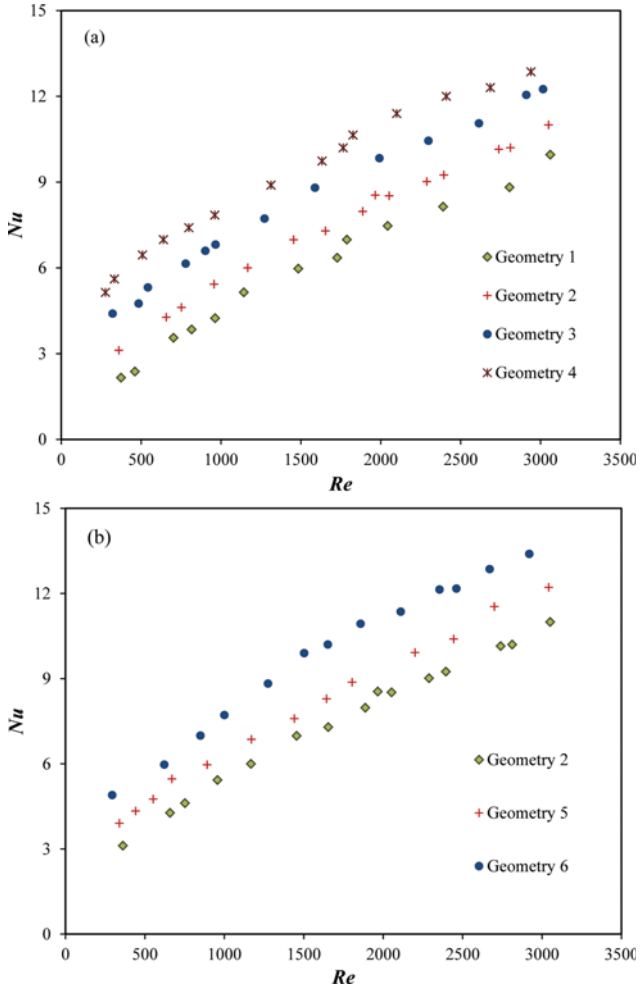

Fig. 6. The effects of (a) curvature radius and (b) straight length between bends on Nusselt number for the serpentine micro-tubes.

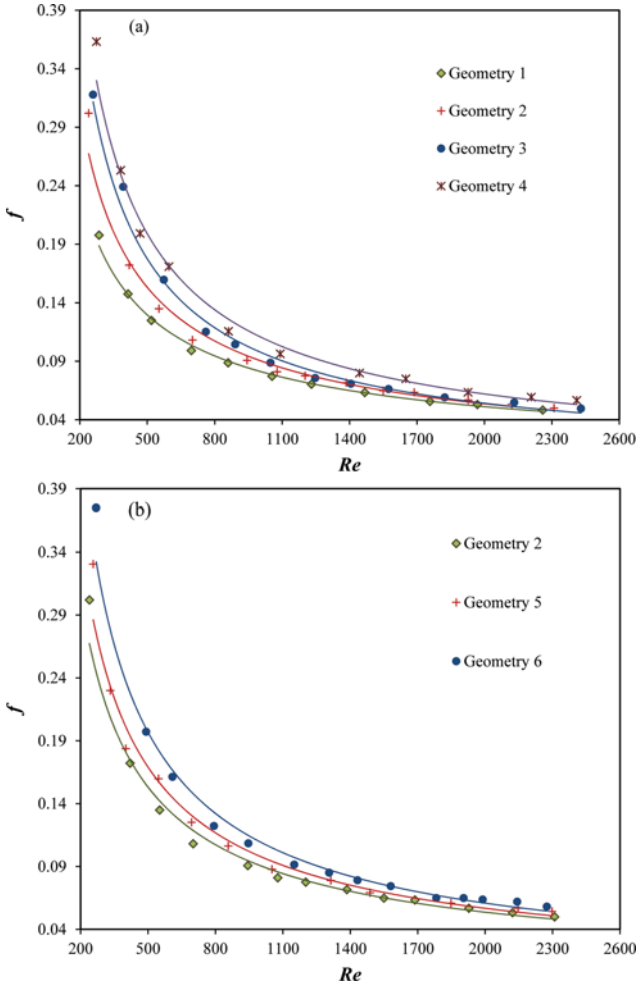

Fig. 7. The effects of (a) curvature radius and (b) straight length between bends on friction factor for the serpentine micro-tubes (solid lines: trend line).

parameters were studied. The measured temperatures, pressures and flow rates were used for calculation of Nu and f. Fig. 6 illustrates the variations of Nusselt number with Reynolds number for the examined serpentine microtubes. Obviously, Nu increases with Re due to increase of convection. In Fig. 6(a) microtubes with same straight length (L_S) and different radius of curvature (R_C) were compared. As can be seen, the Nu is increased with increase in the curvature radius. Higher R_C is associated with higher portions of curved path and the ratio of the bend length to total tube length. The curved bends resulted in higher heat transfer coefficient. The effect of straight length between bends on Nu for tubes with equivalent R_C and various L_S (Geometries 2, 5, and 6) is shown in Fig. 6(b). The Nu decreased with increasing the L_S due to the higher portion of straight passage and further ratio of the straight length to total length of the serpentine microtubes (L_S/L). Figs. 7(a) and (b) illustrate the effects of curvature radius and straight length between bends on friction factor for the studied serpentine microtubes. The friction factor increases with increasing R_C and with decreasing L_S. In general, longer distance between two bends (L_S) causes elongation of the developing length after bends and leads to flow relaxation in the straight length. The shorter distance between bends creates two closer bends and results in reinforcing the strength and rotation of Dean vortices immediately after the bends. Therefore, the pressure drop and heat transfer coefficient increase with decreasing the L_S.

1-1. Thermal-hydraulic Performance Ratio

The thermal-hydraulic performance of the serpentine microtubes was used as a criterion to provide a comparative study on the performance of microtubes. The thermal-hydraulic performance ratio was determined by the Nu and f values for the serpentine and straight microtube as follows [32]:

$$\text{Thermal hydraulic performance ratio} = \frac{\mathrm{Nu}/\mathrm{Nu}_s}{(\mathrm{f}/\mathrm{f}_s)^{(1/3)}} \tag{24}$$

The subscript 's' refers to the straight microtube. A copper microtube with inner diameter of 787.4 μm and 30 cm length was employed in this study. Fig. 8 shows the values of performance ratio for all studied tubes. In general, the results indicate that the performance ratio for all studied serpentine microtubes is more than one. A glance at Fig. 8, confirms that increasing the curvature radius increases the performance ratio. In addition, the performance ratio is increased with decreasing the straight length. Furthermore, the results indicate that the performance slightly decreased by increasing the Reynolds number. This can be explained by the fact that the formed secondary flow in serpentine microtubes was not strong enough to enhance the rate of heat transfer. Therefore, increasing the flow rate of fluid has more significant effect on the pressure losses across the tube than heat transfer rate from it.

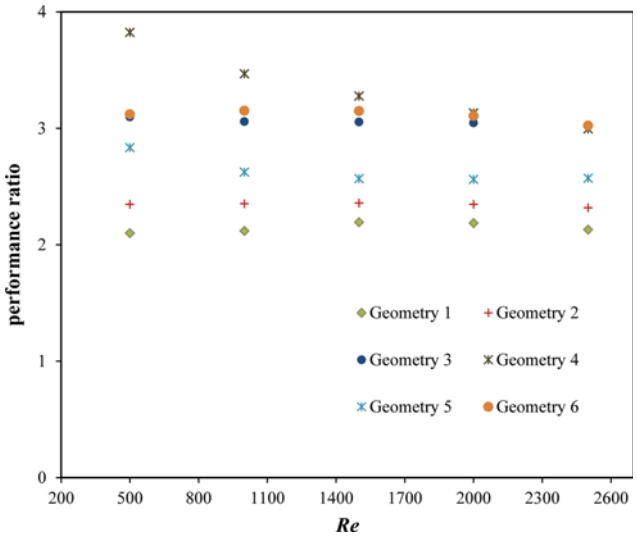

Fig. 8. The performance ratio for the investigated serpentine microtubes.

2. Modeling Results

From the experimental results, it is clear that a change in the geometry of the serpentine microtubes causes simultaneously a change in its thermal and hydrodynamics characteristics. Providing the accurate prediction tool can be used for optimizing the target system, which leads to a trade-off between heat transfer and pressure drop. Developing an accurate prediction model for heat transfer rate and pressure drop can be helpful in the design of this type of heat exchanger. However, the effects of the geometric parameters on the thermal and fluid flow characteristics of them are quite complicated. The adaptive neuro-fuzzy inference system (ANFIS), by applying a large number of parameters, can learn and recognize complicated and nonlinear relations.

In this study, variety of fuzzy inference system structures were generated by using two categories of partitioning methods, which are grid partition and subtractive clustering. The root mean square error (RMSE) function was applied for selecting the best ANFIS structure. In addition, mean relative errors (MRE) were used for evaluating the model performance.

$$\mathrm{RMSE} = \sqrt{\frac{1}{\mathrm{N}}\sum_{i=1}^{N}(\mathrm{t}_i - \mathrm{y}_i)^2} \tag{25}$$

$$\mathrm{MRE}(\%) = \frac{100}{\mathrm{N}}\sum_{i=1}^{N}\left(\frac{|\mathrm{t}_i - \mathrm{y}_i|}{\mathrm{t}_i}\right) \tag{26}$$

where, t is the target (observed) and y is the predicted (model output) value. N is the number of data points. The performance of the developed ANFIS models was determined using a testing data set that was not introduced to the model in the training procedure. All data of geometry 3 and about 30% of data of other geometries proved the validity of the model. Training and test data sets for estimation of Nu were 47 and 34 data samples, respectively. The values for modeling the f were 50 and 34 data values, respectively.

In the first stage, the subtractive clustering method was applied for developing the ANFIS structures. This method has four parameters, including range of influence (ROI), squash factor (SF), accept ratio (AR), and reject ratio (RR). They should be optimized to achieve desired results. We determined the parameters using trial-and-error method in the form done by Cakmakci [33]. Three of the four parameters (ROI, SF, AR, and RR) were held in the constant default values (i.e. ROI=0.5, SF=1.25, AR=0.5, and RR=0.15), then the optimum parameter could be obtained by changing the

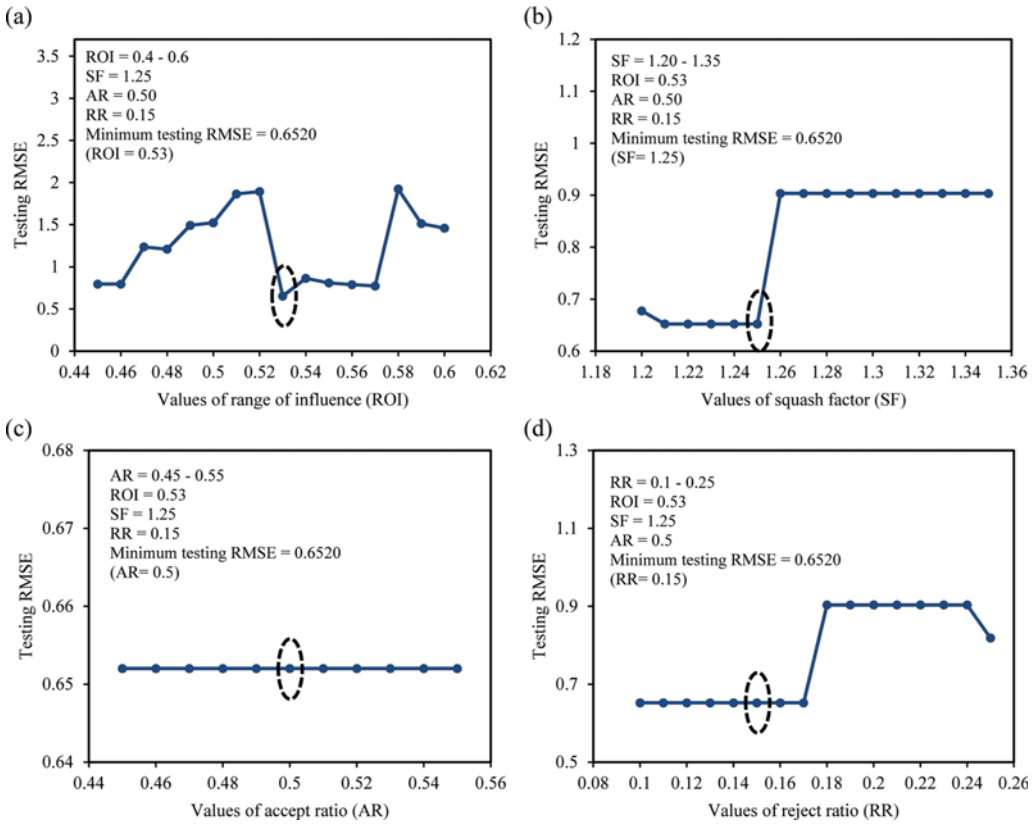

Fig. 9. Effects of clustering parameters on performance of the ANFIS for predicting the Nu.

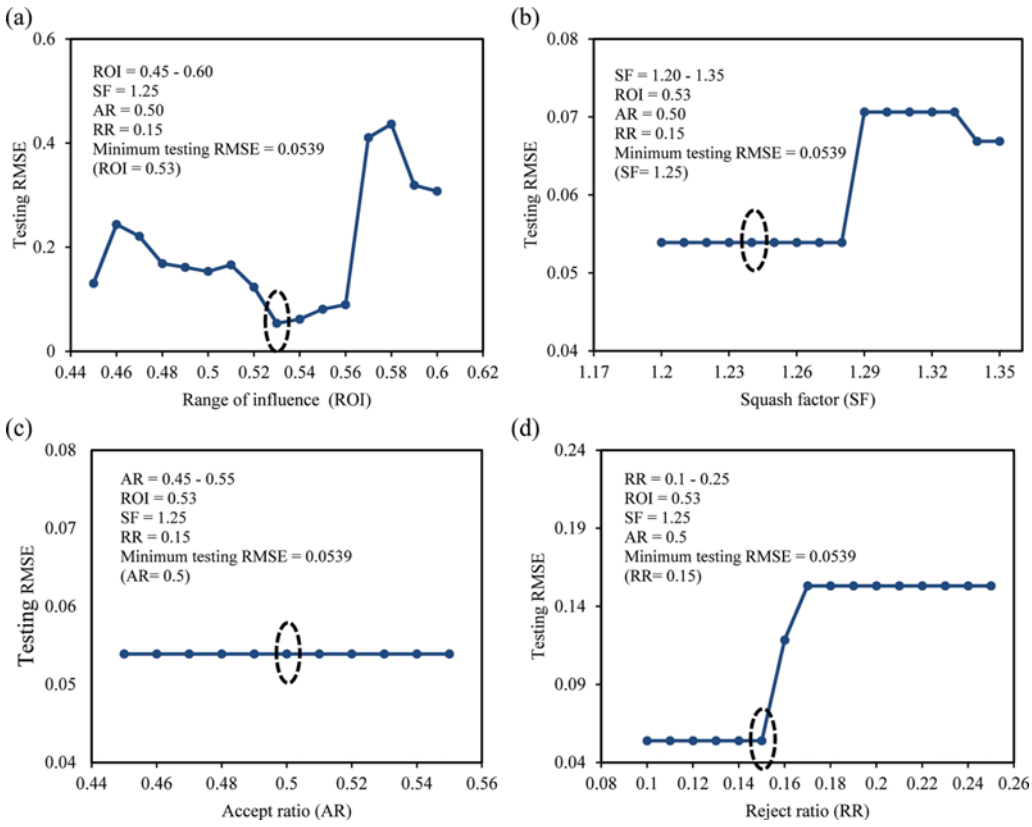

Fig. 10. Effects of clustering parameters on performance of the ANFIS for predicting friction factor.

Table 3. Testing RMSE values of different ANFIS structure for prediction of Nusselt number

Structure number	No. of Mfs[a]	No. of fuzzy rules	MF type					
			Triangular	Trapezoidal	Generalized bell	Gaussian	Combination gaussian	*Π*-shaped
1	2/2/2/2	16	1.9598	0.7064	1.1607	0.4968	0.4349	0.6424
2	3/2/2/2	24	1.4304	1.5605	1.9837	2.1880	1.7831	2.0794
3	2/3/2/2	24	4.0562	4.6167	1.6532	0.4664	1.6183	4.6267
4	2/2/3/2	24	0.9192	1.0048	0.5262	0.4999	0.4159	0.6010
5	2/2/2/3	24	0.6959	1.6801	2.4138	0.9965	0.5504	2.8734
6	3/3/2/2	36	1.7670	12.0216	11.1145	10.0396	15.3831	4.7832
7	2/3/3/2	36	2.7416	3.4675	3.2283	1.0585	1.1500	4.1678
8	2/2/3/3	36	0.8489	2.1114	2.0057	6.5485	0.3166	3.1814
9	3/2/3/2	36	1.4164	0.5937	1.7928	2.5287	1.6397	2.4518
10	2/3/2/3	36	1.4866	2.0845	1.9633	1.9638	2.7225	1.7602
11	2/3/3/3	54	1.5673	1.8961	2.7108	2.4624	2.6105	2.3015
12	3/2/3/3	54	0.6432	1.2450	0.6448	0.6674	1.1081	2.4197
13	3/3/2/3	54	0.9389	2.4034	2.0222	3.2465	1.6772	2.3058
14	3/3/3/2	54	2.7396	2.3869	11.8378	10.5747	1.6322	3.3459
15	3/3/3/3	81	0.8627	2.3870	2.3229	2.5585	1.6590	2.4813
16	4/3/3/3	108	1.2220	1.9751	1.0728	1.1900	2.0100	2.2459
17	3/4/3/3	108	4.0651	4.0729	3.5799	3.5487	4.0701	4.0725
18	3/3/4/3	108	0.8646	2.3870	2.3697	2.5039	1.6594	2.4813
19	3/3/3/4	108	5.4797	20.4937	4.8445	4.5226	2.7152	10.2573

[a]MF1/MF2/MF3/MF4

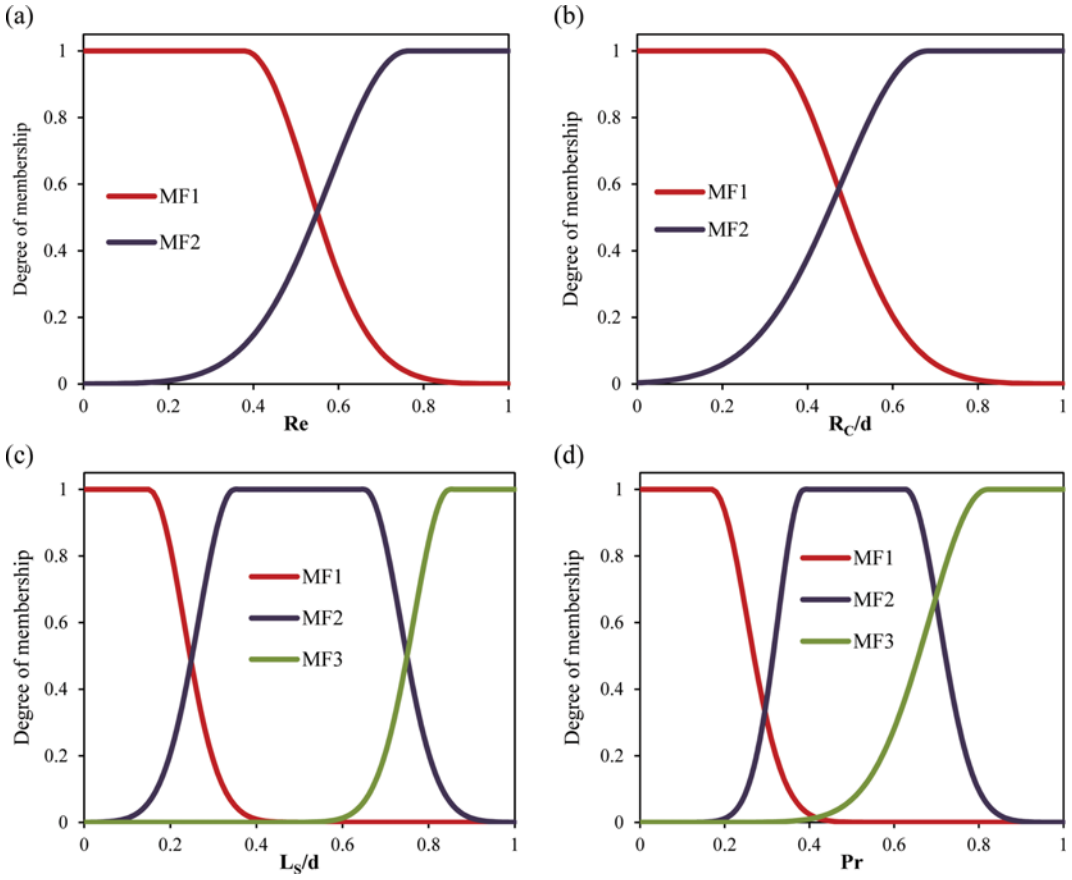

Fig. 11. Fuzzy sets of the input variables for Nu (for normalized input-output data).

value of the fourth parameter around its default value. The best performance was determined based on lowest RMSE value for testing data set. In the first step, the ROI value was determined by examining the model performance for different ROI values. The ROI was changed in the range of 0.45-0.60 while other clustering parameters (SF, AR, and RR) were kept at constant values. In later stages, the optimal value of each particular parameter, which was obtained in a previous test, was employed in the next test. The ranges of 1.2-1.35, 0.45-0.55, and 0.1-0.25 were used for SF, AR, and RR, respectively. Figs. 9 and 10 show the variations in RMSE for testing data set with various clustering parameters for Nu and f modeling, respectively. As can be seen, ANFIS performance was significantly affected by all model parameters except AR values. The results show that the optimum ANFIS configurations for both models are considered by ROI=0.53 and default values for SF, AR, and RR. The minimum testing RMSE values of 0.652 and 0.0539 were obtained for Nu and f ANFIS modeling, respectively.

In addition to the subtractive clustering, the grid partition method was used for finding the best ANFIS structure. In this method, a number of membership function (MF) types including triangular, trapezoidal, Generalized bell, Gaussian, combination Gaussian, and *Π*-shaped were examined. As much as the user can choose the optimum number of rules and MF types, the trial-and-error technique was used for determining the best ANFIS structure. All the mentioned MFs and several structures were examined and a model with minimum testing RMSE was selected. The performances of different ANFIS structure for modeling the Nusselt number in serpentine microtubes are listed in Table 3. ANFIS with 2, 2, 3, and 3 MFs for first, second, third, and fourth input variables, respectively, has minimum testing RMSE (0.3166). The combination Gaussian membership function leads to the best result. The related fuzzy sets of the four input variables are illustrated in Fig. 11. In general, the results show that the neuro-fuzzy networks with more MFs and fuzzy rules resulted in complicated networks, while the model became less accurate. Details of the testing data set, which was used for demonstrating the Nu model validation, are tabulated in Table 4. The low deviation values (MRE and RMSE) for all six examined microtubes verify the model validity, especially for geometry 3, which all corresponding data were not introduced to the model during the learning procedure. Fig. 12 obviously illustrates a desirable agreement between experimental Nu with the one estimated by the corresponding ANFIS. In this figure, it is clear that the deviation (MRE) of all test data points is lower than 15%. Table 5 shows the performance of investigated

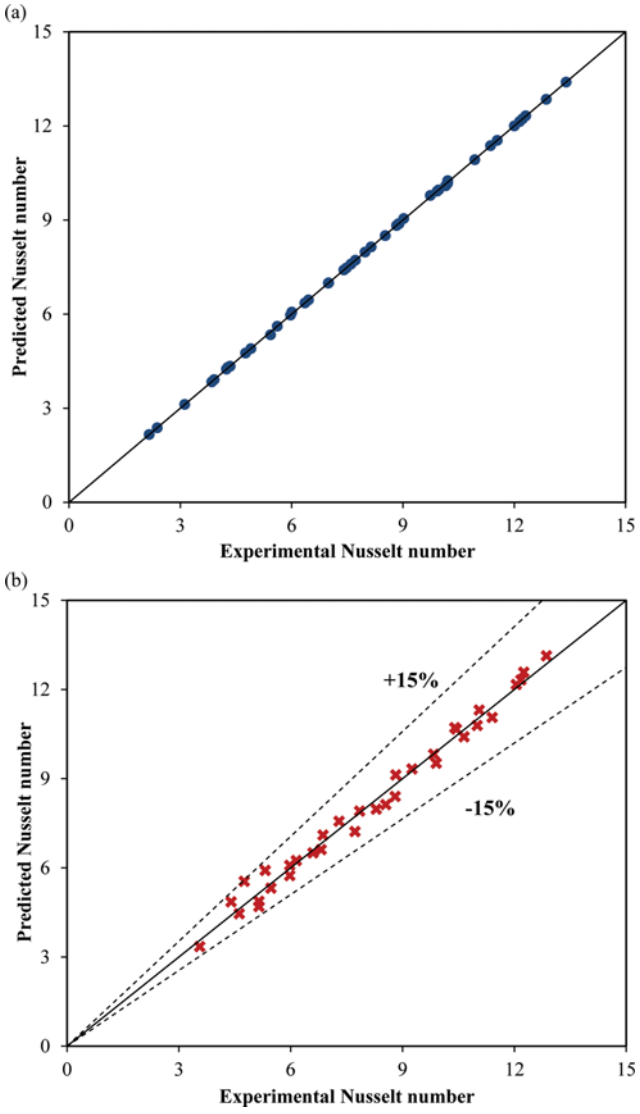

Fig. 12. Comparison between the predicted Nusselt number using ANFIS model and experimental data for (a) train and (b) test data set.

structures of the ANFIS model for predicting the friction factor in the studied serpentine microtubes. The presented structures have three dimensionless input variables (Re, R_C/d, and L_S/d). The results show that ANFIS with structure of 4/2/2 and 16 fuzzy rules leads to a more accurate model. The more complex models have

Table 4. Details of the testing data for Nu

Geometry number	Range of Reynolds number	No. of data points	No. of testing data	Testing RMSE	Testing MRE (%)
1	374.2-3061.7	13	4	0.3127	2.34
2	361.0-3051.1	15	5	0.2551	1.72
3	322-3016.4	13	13 (All data)	0.3830	2.21
4	277.3-2940.0	14	4	0.2491	1.68
5	339.2-3042.0	13	4	0.2656	1.81
6	294.7-2920.3	13	4	0.2517	1.51

Table 5. Testing RMSE values of different ANFIS structure for prediction of friction factor

Structure number	No. of Mfs[a]	No. of fuzzy rules	MF type					
			Triangular	Trapezoidal	Generalized bell	Gaussian	Combination gaussian	*Π*-shaped
1	2./2/2	8	0.01833	0.03991	0.00710	0.00837	0.05133	0.06769
2	3/2/2	12	0.01954	0.00899	0.01582	0.01582	0.01953	0.03030
3	2/3/2	12	0.04666	0.02191	0.00879	0.00879	0.03217	0.04053
4	2/2/3	12	0.0187	0.02162	0.00695	0.00949	0.06005	0.06557
5	2/3/3	18	0.04059	0.02063	0.01088	0.01313	0.03644	0.03430
6	3/2/3	18	0.01955	0.01054	0.00865	0.01129	0.02725	0.02706
7	3/3/2	18	0.11399	0.01377	0.00948	0.01261	0.02567	0.01391
8	3/3/3	27	0.10701	0.01491	0.00835	0.00966	0.03173	0.04213
9	4/2/2	16	0.01724	0.00603	0.01376	0.01193	0.01900	0.04370
10	2/4/2	16	0.06920	0.06649	0.05613	0.05667	0.06597	0.06560
11	2/2/4	16	0.01866	0.02162	0.00782	0.00951	0.06005	0.06557
12	2/4/4	32	0.06909	0.06603	0.05601	0.05786	0.06612	0.06564
13	4/2/4	32	0.01589	0.00844	0.01320	0.01160	0.04737	0.01413
14	4/4/2	32	0.06930	0.06551	0.05215	0.06860	0.06718	0.06464
15	3/4/4	48	0.06492	0.06543	0.05347	0.05639	0.07035	0.07205
16	4/3/4	48	0.02939	0.01626	0.00999	0.01081	0.01081	0.03201
17	4/4/3	48	0.06758	0.06576	0.05309	0.05614	0.06991	0.07067
18	4/4/4	64	0.06753	0.06576	0.05225	0.05607	0.05607	0.07067
19	5/4/4	80	0.06709	0.06823	0.05217	0.05217	0.06719	0.07138
20	4/5/4	80	0.05738	0.06552	0.05899	0.06169	0.06946	0.07066
21	4/4/5	80	0.06708	0.06585	0.05226	0.05624	0.06990	0.07066

[a]MF1/MF2/MF3

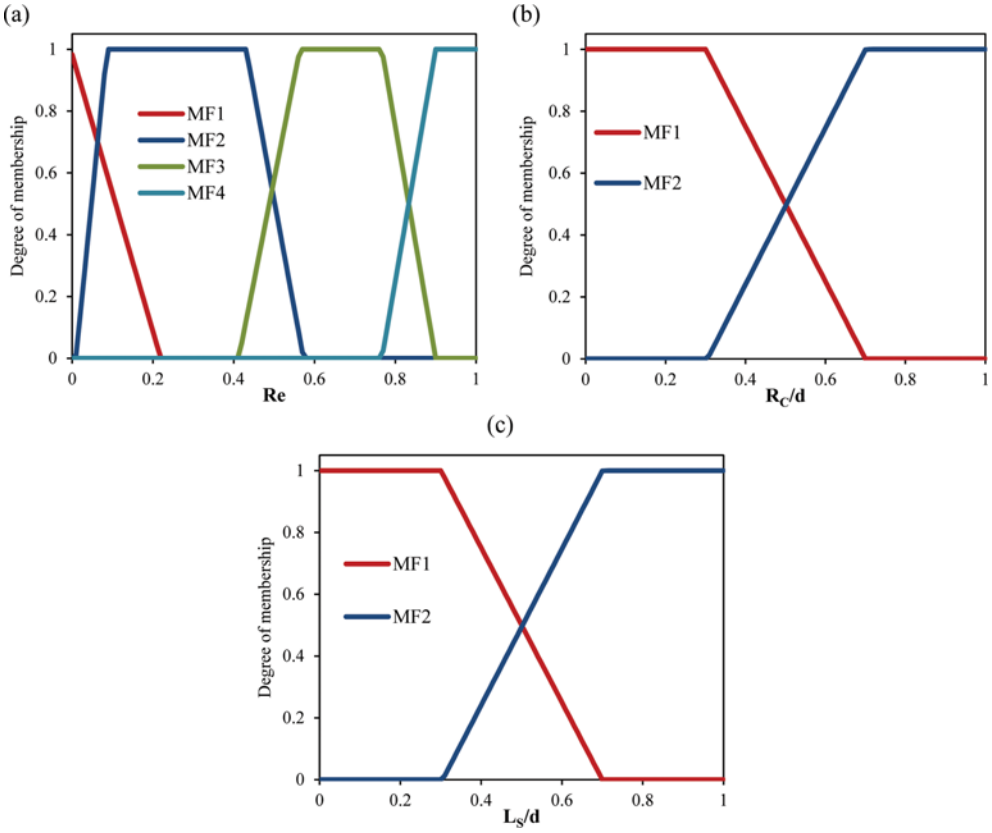

Fig. 13. Fuzzy sets of the input variables for predicting f (for normalized input-output data).

Table 6. Details of the testing data for friction factor

Geometry number	Range of Reynolds number	No. of data points	No. of testing data	Testing RMSE	Testing MRE (%)
1	285.3-2786.2	13	4	0.00495	2.12
2	239.4-2705.0	15	4	0.00235	1.64
3	259.1-2941.8	14	14 (All data)	0.00686	2.04
4	274.1-3100.8	14	4	0.00726	1.46
5	256.2-3340.9	14	4	0.00662	2.32
6	269.4-2674.8	14	4	0.00422	1.56

lower performance. In addition, the selected ANFIS structure has trapezoidal membership function. The curves of input fuzzy sets are shown in Fig. 13. The ranges of Reynolds number for all geometries and details of the model accuracy for predicting the test data set are listed in Table 6. The model validity is proved by the RMSE of 0.00686 and the MRE of 2.04% for geometry 3, which all related data were considered as test data set. The comparison between the predicted values using the developed neuro-fuzzy model and the experimental data points for train and test data sets is shown in Fig. 14. The solid line shows the perfect fit (predicted equal empirical data). The presented results in this figure show a good agreement between the model outputs and target data. The fuzzy rules of the developed first-order Sugeno inference models and optimal consequent parameters for Nu and f are listed in Tables 7 and 8, respectively.

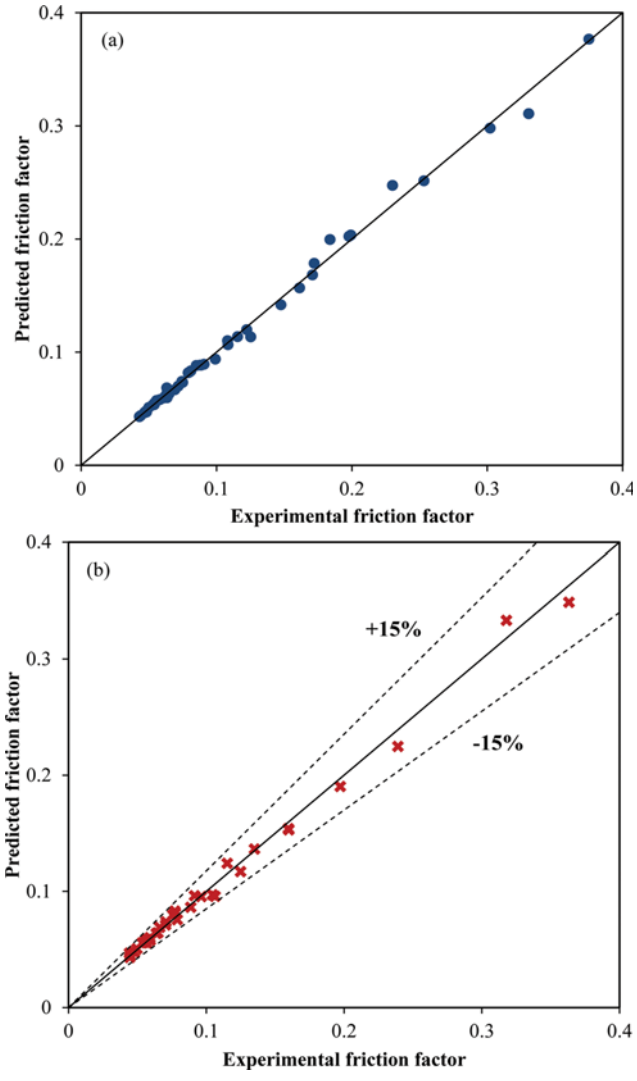

Fig. 14. Comparison between the predicted friction factor using ANFIS model and experimental data for (a) train and (b) test data set.

2-1. Sensitivity Analysis of the System

For artificial intelligence models such as ANFIS and ANN, it is usually impossible to describe the relations that are applied to predict system variables. However, there are some methods that perform a sensitivity analysis using artificial neural networks to indicate the effect of input variables on the outputs of the models [34].In this study, two ANNs with ten and eight hidden neurons were developed for modeling Nu and f, respectively. The procedure of developing the feed forward ANN models is described in detail by Beigzadeh et al. [35]. The level of influence of each input variables on the outputs can be determined by the weights of ANNs using the following relation [34]:

$$I_J = \frac{\sum_{m=1}^{m=N_h}\left(\left(W_{jm}^{ih}/\sum_{k=1}^{N_i}\left|W_{km}^{ih}\right|\right)\times\left|W_{mn}^{ho}\right|\right)}{\sum_{k=1}^{k=N_i}\left\{\sum_{m=1}^{m=N_h}\left(\left(\left|W_{km}^{ih}\right|/\sum_{k=1}^{N_i}\left|W_{km}^{ih}\right|\right)\times\left|W_{mn}^{ho}\right|\right)\right\}} \quad (27)$$

In this equation, I_j is the relative influence of the jth input parameter on the output parameter. N_i and N_h are the numbers of neurons in the input and hidden layer, respectively. Moreover, W is the network weight, the superscripts 'i', 'h' and 'o' refer to input, hidden and output layers, respectively. In addition, subscripts 'k', 'm' and 'n' refer to input, hidden and output neurons, respectively.

Fig. 15 illustrates the percentage of influence of input variables on Nu and f calculated by Eq. (27). The results indicate that for both Nusselt number and friction factor, all of the independent variables have strong effect on the model outputs. The Fig. 15(a) shows that the curvature ratio (R_C/d) with a relative importance of 34% is the most influential parameter on Nu. Moreover, according to Fig. 15(b), it is obvious that Reynolds number (Re) influence percentage of 62% has most effect on f.

2-2. Comparison between ANFIS and Power-law Correlations

The classical power-law correlations are usually used in thermal systems for estimating the dimensionless values, such as Nusselt number and friction factor. In the present study, the precision of

Table 7. Fuzzy rule base of the optimum ANFIS configuration for predicting Nu

Rule number	Rule description
1	If (Re is Re MF1) and (Pr is Pr MF1) and (R_C/d is R_C/d MF1) and (L_S/d is L_S/d MF1) then (Nu=0.7298×Re−0.008382×Pr+5.186×10^{-10}×R_C/d+1.646×L_S/d−0.02515)
2	If (Re is Re MF1) and (Pr is Pr MF1) and (R_C/d is R_C/d MF1) and (L_S/d is L_S/d MF2) then (Nu=3.508×Re−0.07746×Pr+0.002516×R_C/d−1.259×L_S/d−0.2324)
3	If (Re is Re MF1) and (Pr is Pr MF1) and (R_C/d is R_C/d MF1) and (L_S/d is L_S/d MF3) then (Nu=0.5226×Re+0.2318×Pr+0.007276×R_C/d+0.3038×L_S/d+0.6954)
4	If (Re is Re MF1) and (Pr is Pr MF1) and (R_C/d is R_C/d MF2) and (L_S/d is L_S/d MF1) then (Nu=0.000138×Re−1.59×10^{-6}×Pr−3.736×10^{-7}×R_C/d+0.0003108×L_S/d−5.087×10^{-6})
5	If (Re is Re MF1) and (Pr is Pr MF1) and (R_C/d is R_C/d MF2) and (L_S/d is L_S/d MF2) then (Nu=1.073×Re+0.09746×Pr+0.1096×R_C/d−0.4014×L_S/d+0.2923)
6	If (Re is Re MF1) and (Pr is Pr MF1) and (R_C/d is R_C/d MF2) and (L_S/d is L_S/d MF3) then (Nu=1.307×Re+0.282×Pr+0.3169×R_C/d−1.181×L_S/d+0.8454)
7	If (Re is Re MF1) and (Pr is Pr MF1) and (R_C/d is R_C/d MF3) and (L_S/d is L_S/d MF1) then (Nu=0.0003974×Re−0.0001407×Pr−0.002072×R_C/d−0.001192×L_S/d−0.002072)
8	If (Re is Re MF1) and (Pr is Pr MF1) and (R_C/d is R_C/d MF3) and (L_S/d is L_S/d MF2) then (Nu=1.218×Re+0.1108×Pr−0.1213×R_C/d+0.5331×L_S/d−0.1213)
9	If (Re is Re MF1) and (Pr is Pr MF2) and (R_C/d is R_C/d MF3) and (L_S/d is L_S/d MF3) then (Nu=1.061×Re+1.19×Pr−0.8579×R_C/d+1.908×L_S/d−0.8579)
10	If (Re is Re MF1) and (Pr is Pr MF2) and (R_C/d is R_C/d MF1) and (L_S/d is L_S/d MF1) then (Nu=0.1685×Re−0.001936×Pr+1.198×10^{-10}×R_C/d+0.3801×L_S/d−0.005808)
11	If (Re is Re MF1) and (Pr is Pr MF2) and (R_C/d is R_C/d MF1) and (L_S/d is L_S/d MF2) then (Nu=0.81×Re−0.01789×Pr−0.0005811×R_C/d−0.2908×L_S/d−0.05367)
12	If (Re is Re MF1) and (Pr is Pr MF2) and (R_C/d is R_C/d MF1) and (L_S/d is L_S/d MF3) then (Nu=0.1207×Re+0.05352×Pr+0.00168×R_C/d+0.07015×L_S/d+0.1606)
13	If (Re is Re MF1) and (Pr is Pr MF2) and (R_C/d is R_C/d MF2) and (L_S/d is L_S/d MF1) then (Nu=0.0001524×Re+2.247×10^{-5}×Pr+2.282×10^{-5}×R_C/d+5.371×10^{-5}×L_S/d+2.173×10^{-5})
14	If (Re is Re MF1) and (Pr is Pr MF2) and (R_C/d is R_C/d MF2) and (L_S/d is L_S/d MF2) then (Nu=0.2478×Re+0.02256×Pr+0.02539×R_C/d−0.09307×L_S/d+0.06758)
15	If (Re is Re MF1) and (Pr is Pr MF2) and (R_C/d is R_C/d MF2) and (L_S/d is L_S/d MF3) then (Nu=0.3014×Re+0.06512×Pr+0.07335×R_C/d−0.2728×L_S/d+0.1954)
16	If (Re is Re MF1) and (Pr is Pr MF2) and (R_C/d is R_C/d MF3) and (L_S/d is L_S/d MF1) then (Nu=0.6306×Re+0.1194×Pr+0.1193×R_C/d−0.09469×L_S/d+0.1193)
17	If (Re is Re MF1) and (Pr is Pr MF2) and (R_C/d is R_C/d MF3) and (L_S/d is L_S/d MF2) then (Nu=−0.2575×Re+0.3064×Pr+0.356×R_C/d−1.834×L_S/d+0.356)
18	If (Re is Re MF1) and (Pr is Pr MF2) and (R_C/d is R_C/d MF3) and (L_S/d is L_S/d MF3) then (Nu=−1.564×Re+0.1943×Pr+0.7288×R_C/d+0.5112×L_S/d+0.7288)
19	If (Re is Re MF2) and (Pr is Pr MF1) and (R_C/d is R_C/d MF1) and (L_S/d is L_S/d MF1) then (Nu=0.6262×Re+0.5771×Pr+5.05×10^{-13}×R_C/d+0.4746×L_S/d+1.731)
20	If (Re is Re MF2) and (Pr is Pr MF1) and (R_C/d is R_C/d MF1) and (L_S/d is L_S/d MF2) then (Nu=1.798×Re−0.1513×Pr−0.002198×R_C/d+0.4236×L_S/d−0.454)
21	If (Re is Re MF2) and (Pr is Pr MF1) and (R_C/d is R_C/d MF1) and (L_S/d is L_S/d MF3) then (Nu=−0.5057×Re−0.104×Pr+0.003629×R_C/d−0.2293×L_S/d−0.3121)
22	If (Re is Re MF2) and (Pr is Pr MF1) and (R_C/d is R_C/d MF2) and (L_S/d is L_S/d MF1) then (Nu=0.0001183×Re+0.000109×Pr−4.926×10^{-8}×R_C/d+8.965×10^{-5}×L_S/d+0.0003271)
23	If (Re is Re MF2) and (Pr is Pr MF1) and (R_C/d is R_C/d MF2) and (L_S/d is L_S/d MF2) then (Nu=−0.1872×Re−0.08507×Pr−0.09574×R_C/d−0.2068×L_S/d−0.2554)
24	If (Re is Re MF2) and (Pr is Pr MF1) and (R_C/d is R_C/d MF2) and (L_S/d is L_S/d MF3) then (Nu=0.6052×Re+0.1404×Pr+0.1581×R_C/d−0.03339×L_S/d+0.4216)
25	If (Re is Re MF2) and (Pr is Pr MF1) and (R_C/d is R_C/d MF3) and (L_S/d is L_S/d MF1) then (Nu=−5.918×10^{-5}×Re−6.685×10^{-5}×Pr−0.0002578×R_C/d+−0.0001279×L_S/d−0.000258)
26	If (Re is Re MF2) and (Pr is Pr MF1) and (R_C/d is R_C/d MF3) and (L_S/d is L_S/d MF2) then (Nu=0.6636×Re+0.3894×Pr+0.1349×R_C/d−0.3559×L_S/d+0.1349)

Table 7. Continued

Rule number	Rule description
27	If (Re is Re MF2) and (Pr is Pr MF1) and (R_C/d is R_C/d MF3) and (L_S/d is L_S/d MF3) then (Nu=0.6297×Re−0.474×Pr−0.1251×R_C/d+0.3382×L_S/d−0.1251)
28	If (Re is Re MF1) and (Pr is Pr MF1) and (R_C/d is R_C/d MF1) and (L_S/d is L_S/d MF1) then (Nu=0.1446×Re+0.1333×Pr+1.166×10^{-13}×R_C/d+0.1096×L_S/d+0.3998)
29	If (Re is Re MF1) and (Pr is Pr MF1) and (R_C/d is R_C/d MF1) and (L_S/d is L_S/d MF2) then (Nu=0.4152×Re−0.03494×Pr−0.0005075×R_C/d+0.09782×L_S/d−0.1048)
30	If (Re is Re MF1) and (Pr is Pr MF1) and (R_C/d is R_C/d MF1) and (L_S/d is L_S/d MF3) then (Nu=−0.1168×Re−0.02402×Pr+0.0008381×R_C/d−0.05295×L_S/d−0.07207)
31	If (Re is Re MF1) and (Pr is Pr MF1) and (R_C/d is R_C/d MF2) and (L_S/d is L_S/d MF1) then (Nu=0.0001256×Re+5.45×10^{-5}×Pr+2.932×10^{-5}×R_C/d+5.248×10^{-5}×L_S/d+0.0001049)
32	If (Re is Re MF1) and (Pr is Pr MF1) and (R_C/d is R_C/d MF2) and (L_S/d is L_S/d MF2) then (Nu=−0.04323×Re−0.01964×Pr−0.02206×R_C/d−0.04773×L_S/d−0.05893)
33	If (Re is Re MF1) and (Pr is Pr MF1) and (R_C/d is R_C/d MF2) and (L_S/d is L_S/d MF3) then (Nu=0.1398×Re+0.03243×Pr+0.03646×R_C/d−0.007772×L_S/d+0.09731)
34	If (Re is Re MF1) and (Pr is Pr MF1) and (R_C/d is R_C/d MF3) and (L_S/d is L_S/d MF1) then (Nu=0.5141×Re+0.1534×Pr+0.1533×R_C/d+0.1662×L_S/d+0.1533)
35	If (Re is Re MF1) and (Pr is Pr MF1) and (R_C/d is R_C/d MF3) and (L_S/d is L_S/d MF2) then (Nu=0.2084×Re+0.1294×Pr+0.3057×R_C/d+0.07924×L_S/d+0.3057)
36	If (Re is Re MF1) and (Pr is Pr MF2) and (R_C/d is R_C/d MF3) and (L_S/d is L_S/d MF3) then (Nu=0.1404×Re−0.1094×Pr−0.3239×R_C/d−0.2443×L_S/d−0.3239)

Table 8. Fuzzy rule base of the optimum ANFIS configuration for predicting friction factor

Rule number	Rule description
1	If (Re is Re MF1) and (R_C/d is R_C/d MF1) and (L_S/d is L_S/d MF1) then (Nu=−4.357×Re+0.3375×R_C/d−0.3724×L_S/d+1.013)
2	If (Re is Re MF1) and (R_C/d is R_C/d MF1) and (L_S/d is L_S/d MF2) then (Nu=−3.245×Re+0.6561×R_C/d+0.3451×L_S/d+0.2025)
3	If (Re is Re MF1) and (R_C/d is R_C/d MF2) and (L_S/d is L_S/d MF1) then (Nu=−0.3397×Re+0.02631×R_C/d−0.02903×L_S/d+0.07894)
4	If (Re is Re MF1) and (R_C/d is R_C/d MF2) and (L_S/d is L_S/d MF2) then (Nu=−2.008×Re+0.2481×R_C/d+0.3615×L_S/d+0.3504)
5	If (Re is Re MF2) and (R_C/d is R_C/d MF1) and (L_S/d is L_S/d MF1) then (Nu=−0.5097×Re+0.0964×R_C/d−0.04957×L_S/d+0.2892)
6	If (Re is Re MF2) and (R_C/d is R_C/d MF1) and (L_S/d is L_S/d MF2) then (Nu=−0.4156×Re−0.01684×R_C/d+0.1301×L_S/d+0.1111)
7	If (Re is Re MF2) and (R_C/d is R_C/d MF2) and (L_S/d is L_S/d MF1) then (Nu=−0.03974×Re+0.007515×R_C/d−0.003864×L_S/d+0.02255)
8	If (Re is Re MF2) and (R_C/d is R_C/d MF2) and (L_S/d is L_S/d MF2) then (Nu=−0.346×Re+0.08561×R_C/d+0.08447×L_S/d+0.08299)
9	If (Re is Re MF3) and (R_C/d is R_C/d MF1) and (L_S/d is L_S/d MF1) then (Nu=−0.2215×Re+0.05821×R_C/d+0.01679×L_S/d+0.1746)
10	If (Re is Re MF3) and (R_C/d is R_C/d MF1) and (L_S/d is L_S/d MF2) then (Nu=−0.2271×Re+0.05071×R_C/d+0.07682×L_S/d+0.08324)
11	If (Re is Re MF3) and (R_C/d is R_C/d MF2) and (L_S/d is L_S/d MF1) then (Nu=−0.01727×Re+0.004538×R_C/d+0.001309×L_S/d+0.01361)
12	If (Re is Re MF3) and (R_C/d is R_C/d MF2) and (L_S/d is L_S/d MF2) then (Nu=−0.1646×Re+0.046×R_C/d+0.0534×L_S/d+0.0539)
13	If (Re is Re MF4) and (R_C/d is R_C/d MF1) and (L_S/d is L_S/d MF1) then (Nu=−0.152×Re+0.04×R_C/d+0.045×L_S/d+0.12)
14	If (Re is Re MF4) and (R_C/d is R_C/d MF1) and (L_S/d is L_S/d MF2) then (Nu=−0.02605×Re+0.009187×R_C/d+0.02115×L_S/d+0.03838)

Table 8. Continued

Rule number	Rule description
15	If (Re is Re MF4) and (R_C/d is R_C/d MF2) and (L_S/d is L_S/d MF1) then (Nu=−0.01185×Re+0.003118×R_C/d+0.003508×L_S/d+0.009354)
16	If (Re is Re MF4) and (R_C/d is R_C/d MF2) and (L_S/d is L_S/d MF2) then (Nu=−0.01186×Re+0.008273×R_C/d+0.008363×L_S/d+0.009706)

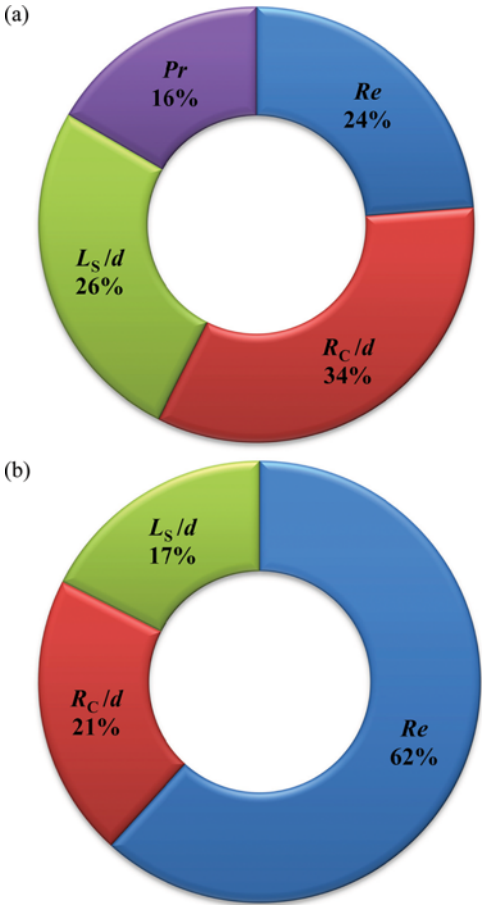

Fig. 15. Importance (%) of the input variables on the (a) Nusselt number and (b) friction factor.

the ANFIS model was compared with empirical power-law correlations. From the experimental measurements of pressure drop and heat transfer rate in the examined serpentine microtubes, new empirical correlations were developed to estimate the Nusselt number and friction factor. For this purpose, the following functional equations were considered:

$$Nu = C_1 Re^{C2} Pr^{C3} \left(\frac{R_C}{d}\right)^{C4} \left(\frac{L_s}{d}\right)^{C5} \quad (28)$$

$$f = C_1 Re^{C2} \left(\frac{R_C}{d}\right)^{C3} \left(\frac{L_s}{d}\right)^{C4} \quad (29)$$

In which, C_i is a constant. The regression equation coefficients were evaluated using the least square method. Consequently, from fitting data the following correlations were obtained:

$$Nu = 0.06 Re^{0.432} Pr^{0.275} \left(\frac{R_C}{d}\right)^{0.778} \left(\frac{L_s}{d}\right)^{-0.176} \quad (30)$$

$$f = 3.537 Re^{-0.792} \left(\frac{R_C}{d}\right)^{0.912} \left(\frac{L_s}{d}\right)^{-0.131} \quad (31)$$

The predicted Nusselt number and friction factor by the proposed correlations were compared with the experimental data. A mean relative error (MRE) of 7.49% was found for Nusselt number, while MRE of 9.76% was obtained for the friction factor. To compare the predicted results by ANFIS models and the developed power-law correlations, the RMSE and MRE values of the models are listed in Table 9. The results indicate that the ANFIS models can estimate Nusselt number and friction factor with a higher precision than those proposed by empirical relations.

In addition, the prediction errors reported in this study are lower than those of relevant works for heat transfer systems. Mehrabi et al. [36] employed the ANFIS model for estimating the heat transfer coefficient and annular pressure drop in helicoidal double-pipe heat exchangers. They obtained RMSE values of 13.612 and 13.815 for heat transfer coefficient and pressure drop, respectively. In another study, the ANFIS modeling of heat transfer of turbulent supercritical carbon dioxide flow in a vertical circular tube was performed by Mehrabi and Pesteei [27]. In their work an RMSE value of 14.267 was obtained for local Nusselt number (Nu_x).

CONCLUSIONS

Two adaptive neuro-fuzzy inference systems (ANFIS) were developed to estimate thermal and flow characteristic in serpentine microtubes. The Nusselt number was modeled as a function of Reyn-

Table 9. Deviations of the selected ANFIS configurations and developed correlations

Method	Stage	Nu			f		
		Data points	MRE (%)	RMSE	Data points	MRE (%)	RMSE
ANFIS	Training	47	0.16	0.0228	50	2.58	0.0055
	Testing	34	3.94	0.3166	34	3.73	0.0060
	Overall	81	1.74	0.2058	84	2.98	0.0056
Power-law Correlation			7.49	0.5381		9.76	0.0144

olds number (Re), Prandtl number (Pr), curvature ratio (R_C/d), and straight length to tube diameter ratio (L_S/d). The friction factor was estimated as a function of Re, R_C/d, and L_S/d. The empirical data were measured and used as input data for the proposed ANFIS models. Grid partition and subtractive clustering methods were employed for developing the ANFIS structure. The results show that the proposed models by grid partition technique have higher performance than that of other one. The high accuracy of the models for estimating the test data set indicates the validity of the methods. In addition, the accuracy of the developed ANFIS models was compared with the corresponding power-law correlations. The results confirmed superior performance of the ANFIS in comparison with the empirical equations.

NOMENCLATURE

A : area [m^2]
C_i : constant
C_p : specific heat capacity [kJ/kg K]
d : tube diameter [m]
h : heat transfer coefficient [W/m^2 K]
f : friction factor
k_f : fluid thermal conductivity [W/m K]
L : tube length [m]
L_S : straight length [m]
M : water mass flow rate [kg/s]
N : number of data points
Nu : Nusselt number
R_C : curvature radius [m]
Re : Reynolds number
t : target data
T : temperature [K]
ΔP : pressure drop [Pa]
V : velocity [m/s]
y : predicted value

Greek Symbols

ν : kinematic viscosity [m^2/s]
ρ : density [kg/m^3]

Subscripts

b : bulk
i : inlet
o : outlet
w : wall

REFERENCES

1. G. M. Mala, D. Li and J. D. Dale, *Int. J. Heat Mass Transfer*, **40**, 3079 (1997).
2. M. R. Kumar and S. Dasgupta, *Chem. Eng. Commun.*, **160**, 225 (1997).
3. M. Dehghan, M. Daneshipour, M. S. Valipour, R. Rafee and S. Saedodin, *Energy Convers. Manage.*, **92**, 244 (2015).
4. M. Shojaeian and S. M. N. Shojaee, *Korean J. Chem. Eng.*, **30**, 823 (2013).
5. S. B. Choi, R. F. Barron and R. O. Warrington, *Actuators, and Systems*, *ASME DSC*, **32**, 123 (1991).
6. C. Hong and Y. Asako, *Appl. Therm. Eng.*, **28**, 1375 (2008).
7. R. Xiong and J. N. Chung, *Int. J. Heat Mass Transfer*, **53**, 3284 (2010).
8. P. F. Hao, X. W. Zhang, Z. H. Yao and F. He, *Exp. Therm. Fluid Sci.*, **32**, 423 (2007).
9. Z. Li, Y. L. He, G. H. Tang and W. Q. Tao, *Int. J. Heat Mass Transfer*, **50**, 3447 (2007).
10. D. Lelea, *Int. Commun. Heat Mass Transfer*, **37**, 245 (2010).
11. W. R. Dean and J. M. Hurst, *Mathematika*, **6**, 77 (1959).
12. W. R. Dean, *Phil. Mag.*, **5**, 673 (1928).
13. S. V. Patankar, V. S. Pratap and D. B. Spalding, *J. Fluid Mech.*, **62**, 539 (1974).
14. C. E. Kalb and J. D. Seader, *Int. J. Heat Mass Transfer*, **15**, 801 (1972).
15. Y. Sui, P. S. Lee and C. J. Teo, *Int. J. Therm. Sci.*, **50**, 2473 (2011).
16. Y. Sui, C. J. Teo, P. S. Lee, Y. T. Chew and C. Shu, *Int. J. Heat Mass Transfer*, **53**, 2760 (2010).
17. N. R. Rosaguti, D. F. Fletcher and B. S. Haynes, *Int. J. Heat Mass Transfer*, **49**, 2912 (2006).
18. Z. Zheng, D. F. Fletcher and B. S. Haynes, *Int. J. Heat Mass Transfer*, **62**, 391 (2013).
19. N. R. Rosaguti, D. F. Fletcher and B. S. Haynes, *Chem. Eng. Technol.*, **28**, 353 (2005).
20. P. E. Geyer, N. R. Rosaguti, D. F. Fletcher and B. S. Haynes, *Microfluid Nanofluid*, **2**, 195 (2006).
21. Z. Zheng, D. F. Fletcher and B. S. Hayne, *Int. J. Heat Mass Transfer*, **71**, 758 (2014).
22. J. S. R. Jang, *IEEE Trans. Syst. Man. Cybern.*, **23**, 665 (1993).
23. M. Mohanraj, S. Jayaraj and C. Muraleedharan, *Renew. Sust. Energ. Rev.*, **16**, 1340 (2012).
24. M. Mohanraj, S. Jayaraj and C. Muraleedharan, *Int. J. Therm. Sci.*, **90**, 150 (2015).
25. A. Mirsepahi, L. Chen and B. O'Neill, *Int. Commun. Heat Mass Transfer*, **41**, 19 (2013).
26. R. Beigzadeh and M. Rahimi, *Int. Commun. Heat Mass Transfer*, **39**, 1647 (2012).
27. M. Mehrabi and S. M. Pesteei, *Int. Commun. Heat Mass Transfer*, **37**, 1546 (2010).
28. J. P. Holman, *Experimental Methods for Engineers*, 3rd Ed. McGraw-Hill, New York (2011).
29. J. Shing and R. Jang, *Adaptive Network, Based Fuzzy Inference*, CiteSeer^x Publication (1993).
30. R. M. Tong, *Automatic*, **13**, 559 (1997).
31. H. Atmaca, B. Cetisli and H. S. Yavuz, The comparison of fuzzy inference systems and neural network approaches with ANFIS method for fuel consumption data, in: Second International Conference on Electrical and Electronics Engineering Papers ELECO'2001, Bursa, Turkey (2001).
32. M. Rahimi, S. R. Shabanian and A. A. Alsairafi, *Chem. Eng. Process.*, **48**, 762 (2009).
33. M. Cakmakci, *Bioproc. Biosyst. Eng.*, **30**, 349 (2007).
34. G. D. Garson, *AI Expert*, **6**, 47 (1991).
35. R. Beigzadeh, M. Rahimi and S. R. Shabanian, *Fluid Phase Equilib.*, **331**, 48 (2012).
36. M. Mehrabi, S. M. Pesteei and T. Pashaee G., *Int. Commun. Heat Mass Transfer*, **38**, 525 (2011).